

**SNX**

**Swiss-Norwegian Foundation for Research with X-Rays**

---

*Report 2021*



## Contents

General Remarks .....	4
Introduction .....	5
Scientific highlights .....	6
New information from XANES/EXAFS for the development of novel ammonia decomposition catalysts .....	7
Intermediate phases of $\text{CH}_3\text{NH}_3\text{PbI}_3$ and their application in X-ray photodetectors .....	10
Unlocking the potential of molecule-based magnets above room temperature .....	12
Scientific output Impact Factors .....	15
Scientific output Research Areas .....	16
Publication list 2021 .....	17
Summary of the works.....	23

## General Remarks

The year 2021 is the eighteenth year of the SNX Foundation.

The accounting is supervised by OPTIMA COMPTA, in Seyssinet-Pariset, in Isère, for the two French associations, and by BfB Fidam Fiduciaire in Renens VD for the SNX Foundation. AUDICT FIDUCIAIRE in Lausanne audits the accounts.

These legal frameworks contribute to the smooth running of the collaborations and to the successful scientific work done at the Swiss Norwegian Beam Lines at ESRF.

The activities of the SNX Foundation are carried out at the European Synchrotron Radiation Facility (ESRF) in Grenoble and comprise the operation and up-grade of two beam line branches, called the Swiss-Norwegian Beam Lines (SNBL).

## Introduction

This report covers the year 2021 but first some recent history. Despite the global pandemic the ESRF managed to startup of the new ESRF-EBS source on time and a, albeit severely disrupted, successful restart of the user service in spring 2020 with mostly remote experiments. The SNBL objectives for this period were part of a long-term plan developed in 2017 and presented in the “SNBL 2019-2020 and beyond” document. This document was supported by the Swiss- and Norwegian users, their respective steering committees and approved by the SNX Council. The document was also handed over in 2018 to the funding agencies in both Norway and Switzerland (Research Council of Norway (RCN) and the State Secretariat for Education research and Innovation (SERI)) at that time. For 2020 this plan was successfully executed and incorporates the completion of the phase 1 installation works, the commissioning with EBS and the restart of the user program. Moreover 2020 was a record year in terms of publication output for SNBL with a total of 140 publications including one in the main Science and one in the main Nature journal.

The new 4-year contract (2021-2024) period has now successfully started with a new Swiss partner, the École Polytechnique Fédérale de Lausanne (EPFL) and for Norway the Norwegian University of Science and Technology (NTNU). Obviously, the user program continued in 2021, moreover the phase 2 major upgrade program for SNBL has started and will span over 4 years. This plan foresees that on BM01, Bragg diffraction, diffuse and small angle scattering, for single crystal, thin films and powder samples will become available. On BM31 it is planned that the combined diffraction and X-ray absorption experiments setup will be completed with Total Scattering and improvements in time and space resolution for all techniques. Improvements in beamline controls and online data analysis tools are also in the pipeline. The BM01 phase 2 upgrade has moderate cost. The BM31 phase 2 project however has a total investment budget of ~2 Million Euro's. Hence external funding was already applied by the Swiss and Norwegian user communities in the years prior and approved. This budget became available immediately with the new contract in place hence all conditions were united for a fresh restart. 2021 has therefore very much been a development and investment year and the works can be summarized as follows:

- 1)** A full user program was successfully and reliably executed on both beamlines, with a big portion of the experiments in the fall and spring of 2021 still in remote.
- 2)** 73 publications using SNBL data appeared in peer review journals, 13% of SNBL publications has an impact factor above 10 and 54% above impact factor 4.
- 3)** Major design, acquisition, assembly and project planning work has been performed for the phase 2 upgrades on both BM01 and BM31.
- 4)** Outside budget investments comprises a total of 2 million Euros.

## Scientific highlights



# ESRF HIGHLIGHTS 2021



## New information from XANES/EXAFS for the development of novel ammonia decomposition catalysts

**On-demand production of hydrogen from ammonia can be accomplished by combining cobalt and rhenium, resulting in comparable activity to ruthenium, the best catalyst. *In-situ* EXAFS/XANES analyses demonstrate that bimetallic Co-Re species are responsible for the activity. The re-reduction of Co partially oxidised by  $\text{NH}_3$  in the presence of Re coincides with the on-set of activity.**

Ammonia is an attractive sustainable energy carrier due to its high hydrogen content and narrow flammability range [1] enabling the long-term energy storage in chemical bonds versus the short-term storage offered by electrochemical storage. Despite its potential, the implementation of ammonia in the energy landscape relies on the capability of releasing hydrogen on demand, preferably at temperatures aligned to those of fuel cells. Considerable scientific effort is currently focused on developing catalysts to attain this goal. The strategy employed here was the development of bi-metallic ammonia decomposition catalysts combining metals possessing different N-atom adsorption energies following the DFT simulations by Hansgen *et al.* [2] to achieve an optimum binding energy for catalytic performance mimicking the N-adsorption energy of ruthenium, the benchmark catalyst in this process.

$\text{CoRe}_{1.6}$  had comparable hydrogen production to 7 wt.% Ru/CNT (Figure 1a) [3]. While 3-5 nm supported Ru nanoparticles (7 wt.% Ru/CNT) present a considerably higher activity than the unsupported  $\text{CoRe}_{1.6}$  per mol of metal (Figure 1b), a rate orders of magnitude higher is shown by the  $\text{CoRe}_{1.6}$  based upon metallic surface area. Therefore, the active sites in Co-Re might be considerably more active than those in Ru. The low temperature activity is directly related to the intimate Co-Re interaction (Figure 2a and b) with the activity onset related to the contraction of the Re-Co bond distance.

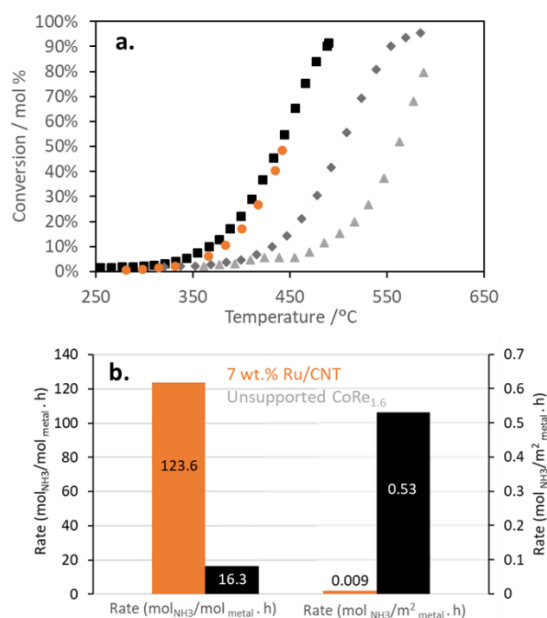


**Fig. 1: a)** Activity of ■  $\text{CoRe}_{1.6}$  ▲  $\text{Ni}_2\text{Mo}_3\text{N}$  ◆  $\text{Co}_3\text{Mo}_3\text{N}$  ● 7% Ru/CNT. **b)** Reaction rate of 7 wt.% Ru/CNT (orange) and  $\text{CoRe}_{1.6}$  (black).

*In-situ* XAS undertaken at **BM31** revealed reduction of the cobalt precursor to  $\text{Co}^0$  occurred over a narrow temperature range from 350°C - 400 °C. Reduction of Re occurred in a single step from 300°C. XANES upon  $\text{NH}_3$  treatment show partial oxidation of cobalt, evident by the increased white line intensity [4] (**Figure 2c**). Although changes were observed in the Co XANES, EXAFS revealed no light atom scattering pairs (i.e., Co-N) were formed during low-temperature  $\text{NH}_3$  treatment. The white line intensity decreased from 400°C during  $\text{NH}_3$  treatment (**Figure 2d** and **e**) and reached a similar intensity to  $\text{CoRe}_{1.6}$  during pre-treatment at 600°C, corresponding to a partial reduction of Co coinciding with the onset of  $\text{NH}_3$  decomposition activity for  $\text{CoRe}_{1.6}$ .

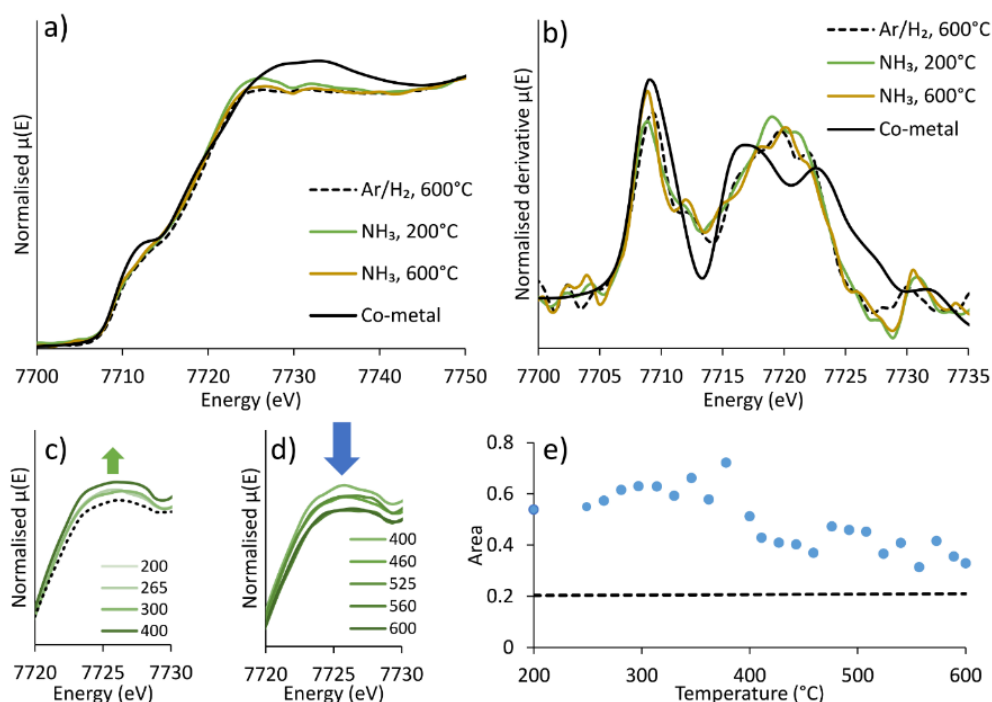


**Fig. 2:** **a)** Co K-edge XANES of  $\text{CoRe}_{1.6}$ . **b)** First derivative of the Co K-edge XANES of  $\text{CoRe}_{1.6}$ . Beginning of 5%  $\text{NH}_3$  treatment (green), end of  $\text{NH}_3$ -decomposition (yellow) and reduced  $\text{CoRe}_{1.6}$  (...). **c)** Co K-edge white line intensity changes during  $\text{NH}_3$ -treatment between 200-400°C (reduced  $\text{CoRe}_{1.6}$  (...)). **d)** Re-reduction of Co between 400-600°C at the Co K-edge. **e)** Area for the Co K-edge white line intensity in  $\text{CoRe}_{1.6}$ .

Despite the changes observed, the Co-Co backscattering pair was stable when the temperature was increased from 300°C to 600 °C under  $\text{NH}_3$ . The average Co-Co multiplicity remained at 4 with a bond distance of 2.45 Å. The Re-Re backscattering pair elongated from 2.65 Å to 2.73 Å during the pre-treatment while a contraction of the bond distance to 2.65 Å occurred after switching from pre-treatment conditions to  $\text{NH}_3$  at 200°C. During  $\text{NH}_3$  decomposition, these distances changed: Re-Re increased to 2.73 Å, while Re-Co was shortened (2.56 Å) coinciding with activity onset. While the change in bond distance of Re-Re approached that of Re-foil (2.74 Å), it did not seem to be associated with sintering of a pure Re-Re phase as the average multiplicity was not changed.

These observations indicate local restructuring of both monometallic and bimetallic particles occurs between 400-600 °C, after  $\text{CoRe}_{1.6}$  is fully reduced. The major contributing species were Co-Co and Re-Re with only ~20% of the bimetallic Re-Co pair. Co-Re is clearly a complex system with interesting  $\text{NH}_3$  decomposition activity, where XANES/EXAFS-derived information is critical for enhanced understanding and further development.

## Principal publication and authors

CO<sub>x</sub>-free hydrogen production from ammonia - mimicking the activity of Ru catalysts with unsupported Co-Re alloys, K. Kirste (a), K.McAulay (b), T.E. Bell (c), D. Stoian (d), S. Laassiri (b,e), A. Daisley (b), J.S.J. Hargreaves (b), K. Mathisen (a), L. Torrente-Murciano (c), *Appl. Catal. B: Environ.* **280**, 119405 (2021); <https://doi.org/10.1016/j.apcatb.2020.119405>.

(a) Norwegian University of Science and Technology (Norway)

(b) University of Glasgow (UK)

(c) University of Cambridge (UK)

(d) ESRF

(e) Mohamed VI Polytechnic University (Morocco)

## References

- [1] T.E. Bell & L. Torrente-Murciano, *Top. Catal.* 59, 1438-1457 (2016).
- [2] D.A. Hansgen *et al.*, *Nat. Chem.* 2, 484-489 (2010).
- [3] A.K. Hill & L. Torrente-Murciano, *Int. J. Hydrog. Energy* 39(15), 7646-7654 (2014).
- [4] F. Carraro *et al.*, *J. Mater. Chem. A* 5, 20808-20817 (2017).

## Intermediate phases of $\text{CH}_3\text{NH}_3\text{PbI}_3$ and their application in X-ray photodetectors

The intermediate phases of the organic-inorganic perovskite crystallisation process and their use in aerosol jet printing (AJP) allows the creation of 3D perovskite structures. Heterostructures based on  $\text{CH}_3\text{NH}_3\text{PbI}_3$  and graphene were successfully manufactured using AJP. X-ray detectors based on such heterostructures demonstrate record-high sensitivity values of  $2.2 \times 10^8 \mu\text{CGy}^{-1}\text{cm}^{-2}$ .

Hybrid organometallic halide perovskites have been intensively investigated in recent years as highly efficient light harvesters for various optoelectronic applications. Nevertheless, there are many open questions remaining regarding their crystallisation process [1]. It is well-known that organic-inorganic perovskite properties are highly affected by external factors such as temperature, pressure, humidity, etc. [2-4]. Therefore, it is crucial to understand the crystallisation process under specific conditions in manufacturing of the devices. Rapid crystallisation of  $\text{CH}_3\text{NH}_3\text{PbI}_3$  ( $\text{MAPbI}_3$ ) is of particular interest, as it is one of the most efficient photovoltaic materials and is in demand for integration into electric circuits. Upon the fast solvent evaporation of saturated  $(\text{DMF}) \cdot (\text{MAPbI}_3)$  solution, yellow micron-long wires appear and then convert to black  $\text{MAPbI}_3$  upon further DMF evaporation.

X-ray diffraction (XRD) data were recorded at beamline **BM01** during the crystallisation process of the wire-shaped  $\text{MAPbI}_3$ . To this end,  $(\text{DMF}) \cdot (\text{MAPbI}_3)$  solution was applied on a glass capillary and XRD data were recorded during evaporation of the solvent. **Figure 1** presents the XRD profiles of the structures that the solution undergoes upon crystallisation. This study shows that, from a soft framework of the inorganic species in solution, the mixture of two intermediate phases appears, and presents a possible transformation process for  $(\text{MA})(\text{DMF})\text{PbI}_3$  into  $\text{MAPbI}_3$ . Such fast-anisotropic crystallisation is important for the printing of  $\text{MAPbI}_3$  for both sensing and emitting light applications.

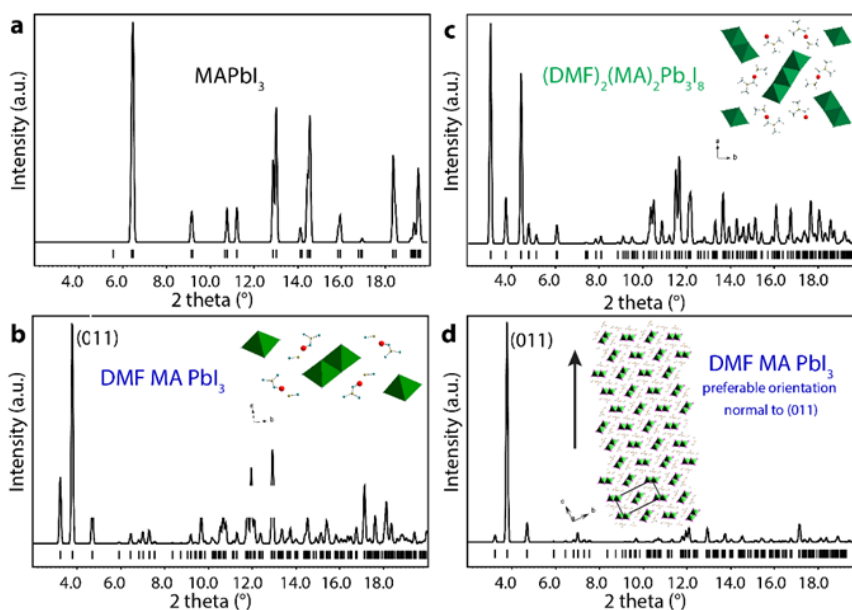


**Fig. 1:** XRD profiles of  $\text{MAPbI}_3$  and intermediate phases. **a-c)** Calculated XRD profiles of  $\text{MAPbI}_3$ ,  $(\text{MA})(\text{DMF})\text{PbI}_3$  and  $(\text{MA})_2(\text{DMF})_2\text{Pb}_3\text{I}_8$  intermediate phases. **d)** XRD profile of  $(\text{MA})(\text{DMF})\text{PbI}_3$  calculated with the preferable grain orientation normal to the (011) planes. *Reproduced from principal publication.*

Aerosol jet printing (AJP) enables the creation of high aspect-ratio crystalline 3D-structures. Devices based on aerosol-jet-printed MAPbI<sub>3</sub> are excellent candidates for X-ray detection, as MAPbI<sub>3</sub> demonstrates strong X-ray-stopping power. The AJP technique also opens the way for the creation of heterostructures of MAPbI<sub>3</sub> with various materials. An X-ray detector unit based on MAPbI<sub>3</sub> on graphene was made, as shown in **Figure 2**.

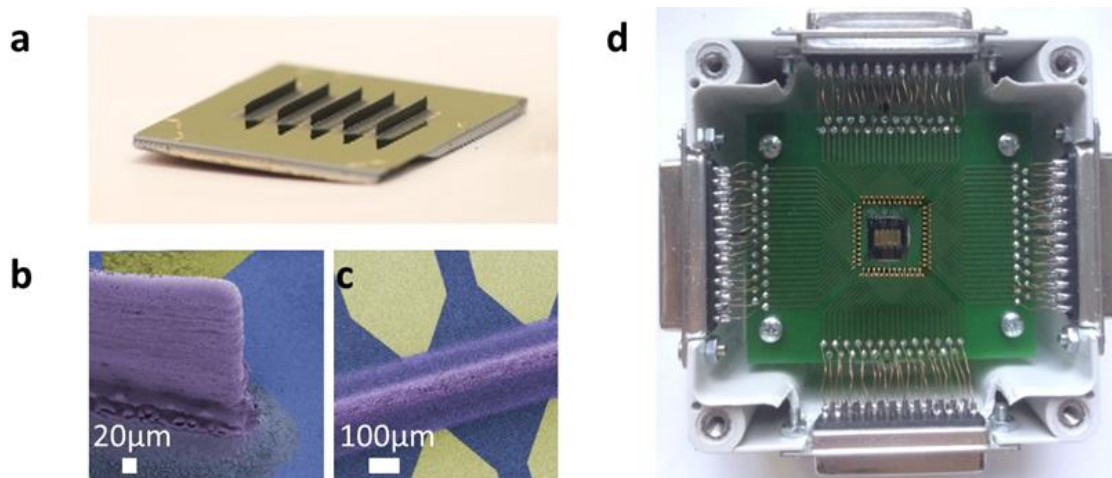


**Fig. 2:** **a)** 1 cm<sup>2</sup> sensing chip with 3D-printed MAPbI<sub>3</sub> walls. **b-c)** False-coloured SEM images of the 3D-printed MAPbI<sub>3</sub> wall on the gold electrodes (graphene in blue, MAPbI<sub>3</sub> in purple and metal electrodes in yellow). **d)** Photograph of the fully integrated X-ray detector unit. *Reproduced from principal publication.*

It was observed that these heterostructures are very promising photoconductors, and the X-ray detector unit demonstrated record sensitivity values of  $2.2 \times 10^8 \mu\text{CGy}^{-1}\text{cm}^{-2}$ . Therefore, such heterostructure-based X-ray detectors could allow for significant lowering of the radiation doses required for X-ray imaging, resulting in safer and more affordable CT imaging systems. With the AJP technique, along with better understanding of the crystallisation processes of complex materials, a new playground for material engineering is opening and new intriguing systems can be created in the future.

### Principal publication and authors

Ultrasensitive 3D Aerosol-Jet-Printed Perovskite X-ray Photodetector, A. Glushkova (a,c), P. Andričević (a), R. Smajda (b), B. Náfrádi (a), M. Kollár (a), V. Djokić (a), A. Arakcheeva (a), L. Forró (a), R. Pugin (b), E. Horváth (a,b), *ACS Nano* **15**, 4077-4084 (2021); <https://doi.org/10.1021/acsnano.0c07993>

(a) *Laboratory of Physics of Complex Matter (LPMC), Ecole Polytechnique Fédérale de Lausanne, Lausanne (Switzerland)*

(b) *Centre Suisse d'Electronique et de Microtechnique (CSEM SA), Neuchatel (Switzerland)*

(c) *Current address: A. Ciers, Department of Microtechnology and Nanoscience (MC2), Chalmers University of Technology, Göteborg (Sweden)*

### References

- [1] K. Mantulnikovs *et al.*, *ACS Photonics* **5**(4), 1476-1485 (2018).
- [2] A. Glushkova *et al.*, *Solar Rrl* **3**(7), 1900044 (2019).
- [3] A. Glushkova *et al.*, *CrystEngComm* **20**(25), 3543-3549 (2018).
- [4] A. Arakcheeva *et al.*, *Acta Cryst. B* **75**(3) 361-370 (2019)

## Unlocking the potential of molecule-based magnets above room temperature

**The thoughtful synthesis of high-performance molecule-based magnets is an ongoing challenge for the scientific community. This work develops a post-synthetic modification strategy, which allows to increase the exchange interactions between the metallic and organic radical spins of pre-formed coordination networks and results in magnets with unprecedented ordering temperatures and coercivity.**

Conventional magnets exhibit several drawbacks due to their purely inorganic origin, such as high energy consumption at fabrication level (e.g., SmCo and AlNiCo) and limited availability of key constituents (e.g., NdFeB and SmCo). While many such drawbacks could, in principle, be solved by using metal-organic magnets, the low operating temperatures of these materials (usually < 77 K) and the lack of generalised synthetic strategies have precluded their use in real-world applications.

With this in mind, this work illustrates the post-synthetic modification of a couple of pre-formed two-dimensional (2D) coordination networks,  $\text{Cr}^{\text{III}}(\text{pyz})_2\text{Cl}_2$  (pyz = pyrazine, ferrimagnet below 55 K) and  $\text{Cr}^{\text{II}}(\text{pyz})_2(\text{OSO}_2\text{CH}_3)_2$  (antiferromagnet below 10 K;  $\text{OSO}_2\text{CH}_3^-$  = methylsulfonate anion) **[1,2]**. The reduction of the organic pyrazine moieties by lithium 1,2-dihydroacenaphthylene ( $\text{Li}^+[\text{C}_{12}\text{H}_{10}^{\bullet-}]$ ) leads to an increase in the number of spins and to strong magnetic interactions between the constituents, resulting in magnets that operate up to 515 K (**Figure 1**). Apart from exceeding the previous record working temperature observed for metal-organic magnets by more than 100 K, these new materials display unprecedented hard magnet properties at room temperature (RT), with coercive fields comparable to those of inorganic magnets.

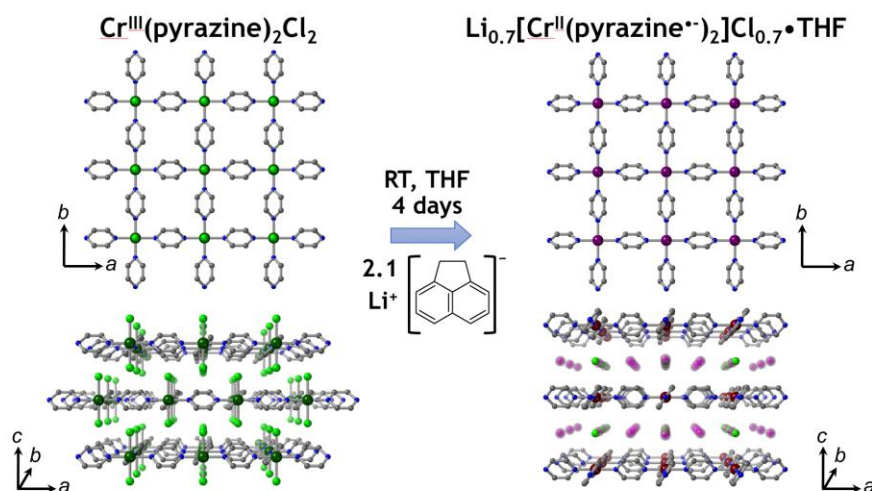


**Fig. 1:** Scheme illustrating the post-synthetic reduction of the pre-formed  $\text{Cr}^{\text{III}}(\text{pyz})_2\text{Cl}_2$  pyrazine-based coordination network. Colour code: C, grey; N, blue;  $\text{Cr}^{\text{III}}$ , dark green;  $\text{Cr}^{\text{II}}$ , dark purple; Cl, light green; Li, purple.

In order to gain insights into these new systems, X-ray absorption spectroscopy (XAS), X-ray magnetic circular dichroism (XMCD) and powder X-ray diffraction (PXRD) experiments were performed at the **ID12** and **BM01** beamlines. X-ray absorption near-edge structure (XANES) spectra collected at the Cr K-edge for the RT magnets and reference compounds revealed the presence of square planar  $\{\text{CrN}_4\}$  environments in the RT magnets (**Figure 2a**), implying the reduction of Cr(III) ions into Cr(II) in the case of  $\text{Cr}^{\text{III}}(\text{pyz})_2\text{Cl}_2$  and the de-coordination of the axial ligands ( $\text{Cl}^-$  and  $^-\text{OSO}_2\text{CH}_3$ ) from the Cr ions. Such findings were further supported by Cr K-edge

extended X-ray absorption fine structure (EXAFS) spectra collected for the chlorine-based RT magnet and, more specifically, by the absence of the characteristic signature of the Cr-Cl bond that appears at  $R \sim 1.9 \text{ \AA}$  in the parent compound (**Figure 2b**).

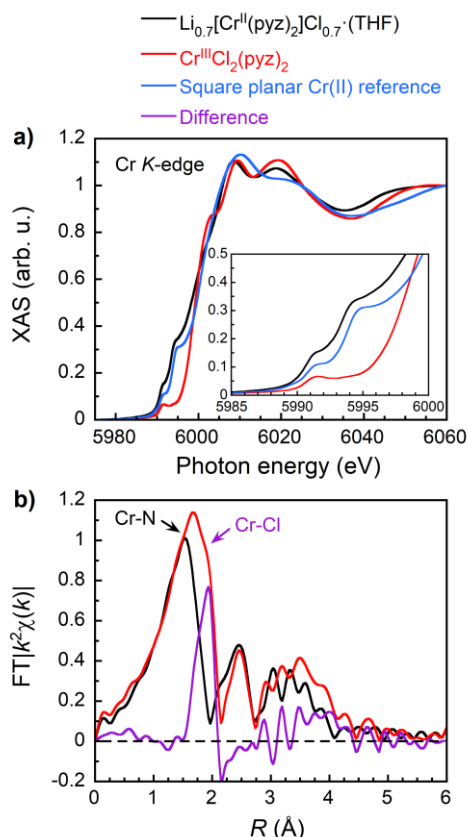


**Fig. 2:** Experimental (a) XANES and (b) FT-EXAFS spectra of  $\text{Li}_{0.7}[\text{Cr}^{\text{II}}(\text{pyz})_2]\text{Cl}_{0.7}\cdot(\text{THF})$  (obtained after post-synthetic reduction of  $\text{Cr}^{\text{III}}(\text{pyz})_2\text{Cl}_2$ ,  $\text{Cr}^{\text{III}}(\text{pyz})_2\text{Cl}_2$  and a square planar Cr(II) model compound at the Cr K-edge at RT.

While structure determination was not possible in the case of the methylsulfonate-based RT magnet due to the co-precipitation of the  $\text{LiOSO}_2\text{CH}_3$  salt, synchrotron X-ray techniques, together with several spectroscopic, thermogravimetric and analytical techniques, revealed that the chlorine-based RT magnet was best described with the  $\text{Li}_{0.7}[\text{Cr}^{\text{II}}(\text{pyz})_2]\text{Cl}_{0.7}\cdot x(\text{THF})$  ( $0.25 \leq x \leq 1$ ) chemical formula, and enabled a good structural model that fit with the experimental PXRD data to be found. Thus,  $\text{Li}_{0.7}[\text{Cr}^{\text{II}}(\text{pyz})_2]\text{Cl}_{0.7}\cdot x(\text{THF})$  consists of quadratic 2D layers composed of  $\text{Cr}^{\text{II}}$  metal ions and radical pyrazine ligands. In addition, 0.7  $\text{Li}^+$ , 0.7  $\text{Cl}^-$  and  $x$  THF molecules per formula unit are located between the layers (**Figure 1**). Interestingly, the unusually strong coercive field of this compound can be modulated from 5300 Oe ( $d_{\text{layers}} = 8.5 \text{ \AA}$ ,  $x = 1$ ) to 7500 Oe ( $d_{\text{layers}} = 7.2 \text{ \AA}$ ,  $x = 0.25$ ) by the amount of THF molecules in the structure, or in other words, by the distance between the layers. Cr K-edge XMCD measurements further support the remarkable magnetic properties of these systems.

In conclusion, this work reports an original methodology to convert pre-formed coordination networks into high-performance magnets. These RT molecule-based magnets are much lighter than the conventional magnets and, therefore, of great relevance to aeronautics and spatial, mobile and wearable technologies.

## Principal publication and authors

Metal-organic magnets with large coercivity and ordering temperatures up to 242°C, P. Perlepe (a,b), I. Oyarzabal (a,c), A. Mailman (d), M. Yquel (a,b), M. Platonov (e), I. Dovgaliuk (e), M. Rouzières (a), P. Négrier (f), D. Mondieig (f), E.A. Suturina (g), M.-A. Dourges (h), S. Bonhommeau (i), R.A. Musgrave (a), K.S. Pedersen (a,i), D. Chernyshov (e), F. Wilhelm (e), A. Rogalev (e), C. Mathonière (b), R. Clérac (a), *Science* **370**, 587-592 (2020); <https://doi.org/10.1126/science.abb3861>

(a) Univ. Bordeaux, CNRS, Centre de Recherche Paul Pascal, UMR 5031, Pessac (France)

(b) Univ. Bordeaux, CNRS, Bordeaux INP, ICMCB, UMR 5026, Pessac (France)

(c) Chemistry Faculty, University of the Basque Country, Donostia-San Sebastián (Spain)

(d) Department of Chemistry, University of Jyväskylä (Finland)

(e) ESRF

(f) Univ. Bordeaux, CNRS, Laboratoire Ondes et Matière d'Aquitaine, UMR 5798, Talence (France)

(g) Department of Chemistry, University of Bath (UK)

(h) Univ. Bordeaux, CNRS, Bordeaux INP, ISM, UMR 5255, Talence (France)

(i) Department of Chemistry, Technical University of Denmark (Denmark)

## References

[1] K.S. Pedersen *et al.*, *Nat. Chem.* **10**, 1056-1061 (2018).

[2] P. Perlepe *et al.*, *Polyhedron* **153**, 248-253 (2018).

## Scientific output Impact Factors

73 peer reviewed papers were published in 2021 containing data from SNBL. >13% of the SNBL publications are published in journals with an impact factor above 10 and % above impact factor 4. See below the full distribution of papers per journal in 2021 and their impact factor.

Journal	Impact Factor	Publications in 2021
ADVANCED MATERIALS	30.849	1
NATURE CHEMISTRY	24.427	1
APPLIED CATALYSIS B-ENVIRONMENTAL	19.503	1
ACS NANO	15.881	1
JOURNAL OF THE AMERICAN CHEMICAL SOCIETY	15.419	1
ANGEWANDTE CHEMIE-INTERNATIONAL EDITION	15.336	1
NATURE COMMUNICATIONS	14.919	1
CHEMICAL ENGINEERING JOURNAL	13.273	1
ACS CATALYSIS	13.084	2
CHEMICAL SCIENCE	9.825	3
ACS APPLIED MATERIALS & INTERFACES	9.229	2
PHYSICAL REVIEW LETTERS	9.161	1
CHEMSUSCHEM	8.928	1
NANO RESEARCH	8.897	1
BATTERIES & SUPERCAPS	7.093	1
CATALYSIS TODAY	6.766	1
CATALYSIS SCIENCE & TECHNOLOGY	6.119	1
INTERNATIONAL JOURNAL OF HYDROGEN ENERGY	5.816	1
JOURNAL OF ALLOYS AND COMPOUNDS	5.316	3
INORGANIC CHEMISTRY	5.165	5
NANOMATERIALS	5.076	1
DALTON TRANSACTIONS	4.39	1
CATALYSTS	4.146	1
JOURNAL OF PHYSICAL CHEMISTRY C	4.126	2
MATERIALS CHEMISTRY AND PHYSICS	4.094	1
CRYSTAL GROWTH & DESIGN	4.076	1
PHYSICAL REVIEW B	4.036	2
FARADAY DISCUSSIONS	4.008	1
PHYSICAL REVIEW MATERIALS	3.989	1
INTERMETALLICS	3.758	1
PHYSICAL CHEMISTRY CHEMICAL PHYSICS	3.676	2
MATERIALS	3.623	1
JOURNAL OF SOLID STATE CHEMISTRY	3.498	3
ACS APPLIED ELECTRONIC MATERIALS	3.314	1
JOURNAL OF SYNCHROTRON RADIATION	2.616	1
CRYSTALS	2.589	2

INORGANICA CHIMICA ACTA	2.545	1
METEORITICS & PLANETARY SCIENCE	2.487	1
ACTA CRYSTALLOGRAPHICA A-FOUNDATION AND ADVANCES	2.29	1
ACTA CRYSTALLOGRAPHICA SECTION B-STRUCTURAL SCIENCE CRYSTAL ENGINEERING AND MATERIALS	2.266	2
ARCHAEOLOGY	1.886	1
MENDELEEV COMMUNICATIONS	1.786	1
HIGH PRESSURE RESEARCH	1.431	1

## Scientific output Research Areas

All the SNBL papers in 2021 were also classified by research area. As the earlier years it's clear SNBL has a strong portfolio in chemistry and materials science followed by physics and crystallography. See below the full distribution per Research Area.

Research Area	Number of Publications
CHEMISTRY, PHYSICAL	23
MATERIALS SCIENCE, MULTIDISCIPLINARY	22
CHEMISTRY, MULTIDISCIPLINARY	15
CHEMISTRY, INORGANIC & NUCLEAR	11
NANOSCIENCE & NANOTECHNOLOGY	8
PHYSICS, APPLIED	7
CRYSTALLOGRAPHY	6
METALLURGY & METALLURGICAL ENGINEERING	5
PHYSICS, CONDENSED MATTER	4
ENGINEERING, CHEMICAL	3
PHYSICS, MULTIDISCIPLINARY	3
ELECTROCHEMISTRY	2
ENGINEERING, ENVIRONMENTAL	2
PHYSICS, ATOMIC, MOLECULAR & CHEMICAL	2
ARCHAEOLOGY	1
CHEMISTRY, ANALYTICAL	1
CHEMISTRY, APPLIED	1
ENERGY & FUELS	1
ENGINEERING, ELECTRICAL & ELECTRONIC	1
GEOCHEMISTRY & GEOPHYSICS	1
GEOSCIENCES, MULTIDISCIPLINARY	1
GREEN & SUSTAINABLE SCIENCE & TECHNOLOGY	1
INSTRUMENTS & INSTRUMENTATION	1
OPTICS	1

## Publication list 2021

1. Arakcheeva, A., Pattison, P., Chapuis, G., Berger, H., Barisic, N., Forro, L. One-dimensional composite host-guest structure in BaVS<sub>3</sub> *Acta Cryst. section B*, 77, 115-122, 2021
2. Asgari, M., Kochetygov, I., Abedini, H., Queen, W.L. Large anisotropic negative thermal expansion in Cu-TDPAT metal-organic framework: A combined in situ X-ray diffraction and DRIFTS study *Nano Res.*, 14, 404-410, 2021
3. Asgari, M., Streb, A., van der Spek, M., Queen, W.L., Mazzotti, M. Synergistic materials and process development: Application of a metal-organic framework, Cu-TDPAT, in single-cycle hydrogen purification and CO<sub>2</sub> capture from synthesis gas *Chem. Eng. Journal*, 414, 128778, 2021
4. Bakken, K., Blichfeld, A.B., Nylund, I.-E., Chernyshov, D., Glaum, J., Grande, T. and Einarsrud, M.-A. Tailoring Preferential Orientation in BaTiO<sub>3</sub>-based Thin Films from Aqueous Chemical Solution Deposition *Chemistry-Methods*, 2021
5. Bakken, K., Gaukås, N.H., Grendal, O.G., Blichfeld, A.B., Tominaka, S., Ohara, K., Chernyshov, D., Glaum, J., Grande, T., Einarsrud, M.-A. In situ X-ray diffraction studies of the crystallization of K<sub>0.5</sub>Na<sub>0.5</sub>NbO<sub>3</sub> powders and thin films from an aqueous synthesis route *Open Ceramics*, 7, 100147, 2021
6. Balaghi, S.E., Heidari, S., Benamara, M., Beyzavi, H., Patzke, G.R. Fluoride etched Ni-based electrodes as economic oxygen evolution electrocatalysts *International J. of Hydrogen Energy*, 2021
7. Balagurov, A.M., Chernyshov, D., Bosak, A.A., Bobrikov, I.A., Sumnikov, S.V., Golovin, I.S. In-grain phase separation and structural ordering in Fe–Ga alloys seen from reciprocal space *Intermetallics*, 128, 107016, 2021
8. Bernal, F.L.M., Lundvall, F., Kumar, S., Hansen, P-A.S., Wragg, D.S., Fjellvåg, H., Løvvik, O.M. Jahn-Teller active fluoroperovskites ACrF<sub>3</sub> (A=Na<sup>+</sup>,K<sup>+</sup>): Magnetic and thermo-optical properties *Phys. Rev. Materials*, 5, 064420, 2021
9. Bogdanov, N.E., Zakharov, B.A., Chernyshov, D., Pattison, P., Boldyreva, E.V. Phase transition in an organic ferroelectric: glycinium phosphite, with and without X-ray radiation damage *Acta Cryst.*, B77, 365-370, 2021
10. Brennhagen, A., Cavallo, C., Wragg, D.S., Sottmann, J., Kuposov, A.Y., Fjellvåg, H. Understanding the (De)Sodiation Mechanisms in Na-Based Batteries through Operando X-Ray Methods *Batteries & Supercaps*, 4, 1-26, 2021
11. Bugaev, A.L., Usoltsev, O.A., Guda, A.A., Lomachenko, K.A., Brunelli, M., Groppo, E., Pellegrini, R., Soldatov, A.V., van Bokhoven, J.A. Hydrogenation of ethylene over palladium: evolution of the catalyst structure by operando synchrotron-based techniques *Faraday Discussions*, 229, 197-207, 2021
12. Burazer, S., Robeyns, K., Guénée, L., Mali, G., Morelle, F., Ban, V., Klaser, T., Filinchul, Y., Cerny, R., Popovic, J. Quenchable Porous High-Temperature Polymorph of Sodium Imidazolate, *Nalm Cryst. Growth Des.*, 21, 770-778, 2021
13. Castro-Fernández, P., Kausnik, M., Wang, Z., Mance, D. Kountoupi, E., Willinger, E., Abdala, P.M., Copéret, C., Lesage, A., Fedorov, A., Müller, C.R. Uncovering selective and active Ga surface sites in gallia-alumina mixed-oxide propane dehydrogenation catalysts by dynamic nuclear polarization surface enhanced NMR spectroscopy *Chem. Sci.*, 12, 15273-15283, 2021

14. Castro-Fernández, P., Mance, D., Liu, C., Moroz, I.B., Abdala, P.M., Pidko, E.A., Copéret, C., Fedorov, A., Müller, C.R. Propane Dehydrogenation on Ga<sub>2</sub>O<sub>3</sub>-Based Catalysts: Contrasting Performance with Coordination Environment and Acidity of Surface Sites *ACS Catal.*, **11**, 907-924, 2021
15. Cherednichenko, K.A., Le Godec, Y., Solozhenko, V.L. Equations of state of new boron-rich selenides B<sub>6</sub>Se and B<sub>12</sub>Se *High Pressure Research*, **41**, 267-274, 2021
16. Cherednichenko, K.A., Mukhanov, V.A., Kalinko, A., Solozhenko, V.L. High-pressure synthesis of boron-rich chalcogenides B<sub>12</sub>S and B<sub>12</sub>Se *J. of Alloys and Compounds*, 162874, 2021
17. Chernysheva, D.V., Leontyev, I.N., Avramenko, M.V., Lyanguzov, N.V., Grebenyuk, T.I., Smirnova, N.V. One step simultaneous electrochemical synthesis of NiO/multilayer graphene nanocomposite as an electrode material for high performance supercapacitors *Mendeleev Commun.*, **31**, 160-162, 2021
18. Chernyshov, D., Dyadkin, V., Emerich, H., Valkovskiy, G., McMonagle, C. J., Van Beek, W. On the resolution function for powder diffraction with area detectors *Acta Cryst. A* **77**, 497-505, 2021
19. Coates, C.S., Baise, M., Schmutzler, A., Simonov, A., Makepeace, J.W., Seel, A.G., Smith, R.I., Playford, H.Y., Keen, D.A., Siegel, R., Senker, J., Slater, B., Goodwin, A.L. Spin-ice physics in cadmium cyanide *Nat. Commun.*, 2272, 2021
20. Darwich, B.P., Guijarro, N., Cho, H.-H., Yao, L., Monnier, L., Schouwink, P., Mensi, M., Yum, J.-H., Sivula, K. Benzodithiophene-Based Spacers for Layered and Quasi-Layered Lead Halide Perovskite Solar Cells *ChemSusChem*, **14**, 1-10, 2021
21. Dovgaliuk, I., Senkovska, I., Li, X., Dyadkin, V., Filinchuk, Y., Chernyshov, D. Kinetic Barriers and Microscopic Mechanisms of Noble Gas Adsorption by Nanoporous  $\gamma$ -Mg(BH<sub>4</sub>)<sub>2</sub> Obtained by Means of Sub-Second X-Ray Diffraction *Angew. Chem. Int. Ed.*, **60**, 5250-5256, 2021
22. Drozhzhin, O.A., Alekseeva, A.M., Shevchenko, V.A., Chernyshov, D., Abakumov, A.M., Antipov, E.V. Phase Transitions in the "Spinel-Layered" Li<sub>1+x</sub>Ni<sub>0.5</sub>Mn<sub>1.5</sub>O<sub>4</sub> (x = 0, 0.5, 1) Cathodes upon (De)lithiation Studied with Operando Synchrotron X-ray Powder Diffraction *Nanomaterials*, **11**, 1368, 2021
23. Drozhzhin, O.A., Grigoryev, V.V., Alekseeva, A.M., Samigullin, R.R., Aksyonov, D.A., Boytsova, O.V., Chernyshov, D., Shapovalov, V.V., Guda, A.A., Soldatov, A.V., Stevenson, K.J., Abakumov, A.M., Antipov, E.V. Revisited Ti<sub>2</sub>Nb<sub>2</sub>O<sub>9</sub> as an Anode Material for Advanced Li-Ion Batteries *ACS Appl. Mater. Interfaces*, 2021
24. Dutta, R., Thoma, H., Chernyshov, D., Nafradi, B., Masuda, T., Kriele, A., Hutanu, V. Topological Analysis of the Experimental Electron Density in Multiferroic Antiferromagnet Ba<sub>2</sub>MnGe<sub>2</sub>O<sub>7</sub> *IEEE Transactions on Magnetics*, 2021
25. Duyar, M.S., Gallo, A., Regli, S.K., Snider, J.L., Singh, J.A., Valle, E., McEnaney, J., Bent, S.F., Rønning, M., Jaramillo, T.F. Understanding Selectivity in CO<sub>2</sub> Hydrogenation to Methanol for MoP Nanoparticle Catalysts Using In Situ Techniques *Catalysts*, **11**, 143, 2021
26. Fjellvag, A.S., Fjellvag, O.S., Breard, Y., Sjustad, A.O. Structural disorder and antiferromagnetism in LaNi<sub>1-x</sub>Pt<sub>x</sub>O<sub>3</sub> *J. of Solid State Chem.*, **299**, 122181, 2021
27. Fjellvag, A.S., Fjellvag, O.S., Kumar, S., Ruud, A., Sjustad, A.O. Interplay of valence states and magnetic interactions in the perovskite system LaNi<sub>1-x</sub>Rh<sub>x</sub>O<sub>3</sub> *J. of Solid State Chem.*, **298**, 122124, 2021
28. Glushkova, A., Andricevic, P., Smajda, R., Nafradi, B., Kollar, M., Djokic, V., Arakcheeva, A., Forro, L., Pugin, R., Horvath, E. Ultrasensitive 3D Aerosol-Jet-Printed Perovskite X-ray Photodetector *ACS Nano*, **15**, 4077-4084, 2021

29. Grinderslev, J.B., Andersson, M.S., Trump, B.A., Zhou, W., Udovic, T.J., Karlsson, M., Jensen, T.R. Neutron scattering investigations of the global and local structures of ammine yttrium borohydrides *J. Phys. Chem. C*, 28, 15415-15423, 2021
30. Grinderslev, J.B., Jensen, T.R. Trends in the Series of Ammine Rare-Earth-Metal Borohydrides: Relating Structural and Thermal Properties *Inorg. Chem.*, 4, 2573-2589, 2021
31. Guda, L.V., Kravtsova, A.N., Kubrin, S.P., Guda, A.A., Mazuritskiy, M.I., Tereshchenko, A.A., Popov, Y.V., Soldatov, A.V. Complex diagnostics of ordinary chondrites Markovka, Polujamki, Sayh al Uhaymir 001, Dhofar 020, and Jiddat al Harasis 055 by X-ray techniques and Mössbauer spectroscopy *Meteoritics & Planetary Science*, 56, 12, 2021
32. Heidari, S., Balaghi, S.E., Sologubenko, A.S., Patzke, G.R. Economic Manganese-Oxide-Based Anodes for Efficient Water Oxidation: Rapid Synthesis and In Situ Transmission Electron Microscopy Monitoring *ACS Catal.*, 11, 2511-2523, 2021
33. Jablonka, K.M., Moosavi, S.M., Asgari, M., Ireland, C., Patiny, L., Smit, B. A data-driven perspective on the colours of metal-organic frameworks *Chem. Sci.*, 12, 3587-3598, 2021
34. Jørgensen, M., Lee, Y.-S., Paskevicius, M., Hansen, B.R.S., Jensen, T.R. Synthesis and crystal structures of decahydro-closo-decaborates of the divalent cations of strontium and manganese *J. of Solid State Chem.*, 298, 122133, 2021
35. Jørgensen, M., Zhou, W., Wu, H., Udovic, T.J., Paskevicius, M., Cerny, R., Jensen, T.R. Polymorphism of calcium decahydrido-closo-decaborate and characterizaion of its hydrates *Inorg. Chem.*, 15, 10943-10957, 2021
36. Kamyshova, E., Skorynina, A., Lazzarini, A., Bugaev, A., Olsbye, U., Soldatov, A. X-ray absorption spectroscopy study of metal-organic frameworks functionalized by Pd: Formation and growth of Pd nanoparticles *Acta Cryst.*, A77, C1270, 2021
37. Kartashov, O.O., Chernov, A.V., Polyanichenko, D.S., Butakova, M.A. XAS data reprocessing of nanocatalysts for machine learning applications *Materials*, 14, 7884, 2021
38. Kim, J.-H., Peets, D.C., Reehuis, M., Adler, P., Maljuk, A., Ritschel, T., Allison, M.C., Geck, J., Mardegan, J.R.L., Bereciartua Perez, P.J., Francoual, S., Walters, A.C., Keller, T., Abdala, P.M., Pattison, P., Dosanjh, P., Keimer, B. Hidden Charge Order in an Iron Oxide Square-Lattice Compound *Phys. Rev. Lett.*, 127, 097203, 2021
39. Kim, S.M., Armutlulu, A., Liao, W.-C., Hosseini, D., Stoian, D., Chen, Z., Abdala, P.M., Copéret, C., Müller, C. Structural insight into an atomic layer deposition (ALD) grown Al<sub>2</sub>O<sub>3</sub> layer on Ni/SiO<sub>2</sub>: impact on catalytic activity and stability in dry reforming of methane *Catal. Sci. Technol.*, 11, 7563-7577, 2021
40. Kirste, K.G., McAuley, K., Bell, T.E., Stoian, D., Laassiri, S., Daisley, A., Hargreaves, J.S.J., Mathisen, K., Torrente-Murciano, L. CO<sub>x</sub>-free hydrogen production from ammonia—mimicking the activity of Ru catalysts with unsupported Co-Re alloys *Applied Catal. B: Envir.*, 280, 119405, 2021
41. Klimova, N., Snigireva, I., Snigirev, A., Yefanov, O. Suppressing Diffraction-related intensity losses in transmissive single-crystal X-ray optics *Crystals*, 11, 1561, 2021
42. Klimova, N., Yefanov, O., Snigireva, I., Snigirev, A. Determination of the Exact Orientation of Single-Crystal X-ray Optics from Its Glitch Spectrum and Modeling of Glitches for an Arbitrary Configuration *Crystals*, 11, 504, 2021
43. Kokliukhin, A., Nikulshina, M., Mozhaev, A., Lancelot, C., Lamonier, C., Nuns, N., Blanchard, P., Bugaev, A., Nikulshin, P. Bulk hydrotreating MonW<sub>12</sub>-nS<sub>2</sub> catalysts based on SiMonW<sub>12</sub>n heteropolyacids prepared by alumina elimination method *Catal. Today*, 377, 26-37, 2021

44. Marshall, K.P., Eidem, S.O., Småbråten, D.R., Selbach, S.M., Grande, T., Einarsrud, M.-A. Hydrothermal synthesis of hexagonal YMnO<sub>3</sub> and YbMnO<sub>3</sub> below 250°C Dalton Trans., 50, 9904-9913, 2021
45. Martini, A., Guda, A.A., Guda, S.A., Dulina, A., Tavani, F., D'Angelo, P., Borfecchia, E., Soldatov, A.V. Estimating a set of pure XANES spectra from multicomponent chemical mixtures using a transformation matrix-based approach SPPHY, 220, 65-84, 2021
46. Molchanova, A.D., Prosnikov, M.A., Petrov, V.P., Dubrovin, R.M., Nefedov, S.G., Chernyshov, D., Smirnov, A.N., Davydov, V.Yu., Boldyrev, K.N., Chernyshev, V.A., Pisarev, R.V., Popova, M.N. Lattice dynamics of cobalt orthoborate Co<sub>3</sub>(BO<sub>3</sub>)<sub>2</sub> with kotoite structure J. of Alloys and Compounds, 865, 158797, 2021
47. Nadjafi, M., Kierzkowska, A.M., Armutlulu, A., Verel, R., Fedorov, A., Abdala, P.M., Müller, C.R. Correlating the structural evolution of ZnO/Al<sub>2</sub>O<sub>3</sub> to spinel zinc aluminate with its catalytic performance in propane dehydrogenation J. Phys. Chem. C, 25, 14065-14074, 2021
48. Nikiforova, Y.A., Ivanova, A.G., Frolov, K.V., Lyubutin, I.S., Chareev, D.A., Baskakov, A.O., Starchikov, S.S., Troyan, I.A., Lyubutina, M.V., Naumov, P.G., Abdel-Hafiez, M. Crystal structure and phase transitions at high pressures in the superconductor FeSe<sub>0.89</sub>S<sub>0.11</sub> J. of Alloys and Compounds, 860, 158419, 2021
49. Park, J.G., Collins, B.A., Darago, L.E., Runcevski, T., Ziebel, M.E., Aubrey, M.L., Jiang, H.Z.H., Velasquez, E., Green, M.A., Goodpaster, J.D., Long, J.R. Magnetic ordering through itinerant ferromagnetism in a metal-organic framework Nature Chemistry, 2021
50. Periyasamy, M., Patra, L., Fjellvåg, O.S., Ravindran, P., Sørby, M.H., Kumar, S., Sjøstad, A.O., Fjellvåg, H. Effect of electron doping on the crystal structure and physical properties of an n=3 Ruddlesden-Popper compound La<sub>4</sub>Ni<sub>3</sub>O<sub>10</sub> ACS Appl. Electron. Mater., 6, 2671-2684, 2021
51. Primera Darwich, B., Guijarro, N., Cho, H.-H., Yao, L., Monnier, L., Schouwink, P., Mensi, M., Yum, J.-H., Sivula, K. Benzodithiophene-based spacers for layered and quasi-layered lead halide perovskite solar cells ChemSusChem, 14, 3001, 2021
52. Rasmussen, K.L., Delbey, T., Skytte, L., La Nasa, J., Colombini, M.P., Ravnsbæk, D.B., Jørgensen, B., Kjeldsen, F., Grønnow, B., Larsen, S. In the darkest hour: Analyses of a black spot on the last page of the diary of polar explorer Jørgen Brønlund (d. 1907) Archaeometry, 63, 893-905, 2021
53. Safonov, V.A., Fishgoit, L.A., Safonova, O.V., Glatzel, P. On the presence of covalently bound phosphorus in amorphous Ni-Co-P and Fe-Co-P electroplates Mat. Chem. and Phys., 272, 124987, 2021
54. Scheinost, A.C., Claussner, J., Exner, J., Feig, M., Findeisen, S., Hennig, C., Kvashnina, K.O., Naudet, D., Prieur, D., Rossberg, A., Schmidt, M., Qiu, C., Colomp, P., Cohen, C., Dettona, E., Dyadkin, V., Stumpf, T. ROBL-II at ESRF: a synchrotron toolbox for actinide research J. Synchrotron Rad., 28, 33-349, 2021
55. Skjærvø, S.L., Ong, G.K., Grendal, O.G., Wells, K.H., van Beek, W., Ohara, K., Milliron, D.J., Tominaka, S., Grande, T., Einarsrud M.-A. Understanding the hydrothermal formation of NaNbO<sub>3</sub>: its full reaction scheme and kinetics Inorg. Chem., 11, 7632-7640, 2021
56. Sørli, G., Azim, M.M., Rønning, M., Mathisen, K. Improved lifetime and stability of copper species in hierarchical, copper-incorporated CuSAPO-34 verified by catalytic model reactions Phys. Chem. Chem. Phys., 23, 16785-16794, 2021
57. Steele, J.A., Prakasam, V., Huang, H., Solano, E., Chernyshov, D., Hofkens, J., Roeffaers, M.B.J. Trojans That Flip the Black Phase: Impurity-Driven Stabilization and Spontaneous Strain Suppression in γ-CsPbI<sub>3</sub> Perovskite J. Am. Chem. Soc., 143, 28, 2021

58. Steele, J.A., Solano, E., Jin, H., Prakasam, V., Braeckvelt, T., Yuan, H., Lin, Z., de Kloe, R., Wang, Q., Rogge, S.M., van Speybroeck, V., Chernyshov, D., Hofkens, J., Roeffaers, M.B.J. Texture Formation in Polycrystalline Thin Films of All-Inorganic Lead Halide Perovskite *Advanced Materials*, 33, 13, 2021
59. Stehle, M., Gaur, A., Weber, S., Sheppard, T.L., Thomann, M., Fischer, A., Grunwaldt, J.-D. Complementary operando insights into the activation of multicomponent selective propylene oxidation catalysts *J. of Catalysis*, in Press, 2021
60. Stingaciu, M., Mishra, D., Fernandez, C.d.J., Cabassi, R., Eikeland, A.Z., Christensen, M., Deledda, S. High magnetic coercive field in Ca-Al-Cr substituted strontium hexaferrite *J. of Alloys and Compounds*, 883, 160768, 2021
61. Sungmin, K., Andac, A., Liao, W.-C., Hosseini, D., Stoian, D., Chen, Z., Abdala, P.M., Copéret, C., Müller, C.R. Structural insight into an atomic layer deposition (ALD) grown Al<sub>2</sub>O<sub>3</sub> layer on Ni/SiO<sub>2</sub>: impact on catalytic activity and stability in dry reforming of methane *ChemRxiv*, 2021
62. Suresh, L., Finstad, J., Törnroos, K.W., Le Roux, E. Bis(phenolate)-functionalized N-heterocyclic carbene complexes of oxo- and imido-vanadium(V) *Inorganica Chimica Acta*, 521, 120301, 2021
63. Tran, M.K., Akrap, A., Levallois, J., Teyssier, J., Schouwink, P., Besnard, C., Lerch, P., Allen, J.W., Greenblatt, M., van der Marel, D. Pressure-induced structural transitions triggering dimensional crossover in the lithium purple bronze Li<sub>0.9</sub>Mo<sub>6</sub>O<sub>17</sub> *Phys. Rev. B*, 103, 235124, 2021
64. Tsoukalou, A., Serykh, A.I., Willinger, E., Kierzkowska, A., Abdala, P.M., Fedorov, A., Müller, C.R. Hydrogen dissociation sites on indium-based ZrO<sub>2</sub>-supported catalysts for hydrogenation of CO<sub>2</sub> to methanol *Catal. Today*, In Press, 2021
65. Udoenko, S., Filimonov, A., Vakhrushev, S., Chernyshov, D., Loginov, B., Karev, P. A system for simultaneous application of uniaxial strain and electric field to the crystal sample in wide temperature range for x-ray scattering experiments 2021 *International Conference on Electrical Engineering and Photonics (EExPolytech)*, 146-148, 2021
66. Vakhrushev, S. B., Andronikova, D., Bronwald, I., Koroleva, E. Yu., Chernyshov, D., Filimonov, A. V., Udoenko, S. A., Rudskoy, A. I., Ishikawa, D., Baron, A. Q. R., Bosak, A., Leontiev, I. N., Tagantsev, A.K. Electric field control of antiferroelectric domain pattern *Phys. Rev. B*, 103, 214108, 2021
67. Valverde-Muñoz, F.J, Kazan, R., Boukheddaden, K., Ohba, M., Real, J.A., Delgado, T. Downsizing of nanocrystals while retaining bistable spin crossover properties in three-dimensional Hofmann-type {Fe(pz)[Pt(CN<sub>4</sub>)]-Iodine adducts *Inorg. Chem.*, 12, 8851-8860, 2021
68. Van Smaalen, S., Ramakrishnan, S., Ramakrishnan, S. Atomic mechanisms for the formation of charge-density waves in three-dimensional electronic crystals *Acta Cryst.*, A77, C1234, 2021
69. Varandili, S.B., Stoian, D., Vavra, J., Rossi, K., Pankhurst, J.R., Guntern, Y.T., Lopez, N., Buonsanti, R. Elucidating the structure-dependent selectivity of CuZn towards methane and ethanol in CO<sub>2</sub> electroreduction using tailored Cu/ZnO precatalysts *Chem. Sci.*, 12, 14484-14493, 2021
70. Yakubovich, O.V., Shvanskaya, L.V., Bolotina, N.B., Ivanova, A.G., Kiriukhina, G.V., Dovgaliuk, I.N., Volkov, A.S., Dimitrova, O.V., Vasiliev, A.N. An Orthorhombic Modification of KCoPO<sub>4</sub> stabilized under hydrothermal conditions: Crystal chemistry and magnetic behavior *Inorg. Chem.*, 60, 9461-9470, 2021
71. Zabilskiy, M., Sushkevich, V.L., Newton, M.A., Krumeich, F., Nachtegaal, M., van Bokhoven, J.A. Mechanistic study of carbon dioxide hydrogenation over Pd/ZnO-based catalysts: the role of palladium-zinc alloy in selective methanol synthesis *Ang. Chemie*, 133, 17190-17196, 2021

72. Zavorotynska, O., Sørby, M.H., Vitillo, J.G., Deledda, S., Frommen, C., Hauback, B.C. Experimental and computational characterization of phase transition in CsB<sub>3</sub>H<sub>8</sub> Phys. Chem. Chem. Phys., Advance Article, 2021
73. Zhu, J., Guðmundsdóttir, J.B., Strandbakke, R., Both, K.G., Aarholt, T., Carvalho, P.A., Sørby, M.H., Jensen, I.J.T., Guzik, M.N., Norby, T., Haug, H., Chatzidakis, A. Double perovskite cobaltites integrated in a monolithic and noble metal-free photoelectrochemical device for efficient water splitting ACS Appl. Mater. Interfaces, 17, 20313-20325, 2021

## Summary of the works

The ESRF has started to operate its beamlines with the new Extremely Brilliant Source in 2020. The SNBL has been preparing since 2017 for this event following a plan outlined in the “SNBL 2019-2020 and beyond” document. This document was supported by the Swiss- and Norwegian users, their respective steering committees and approved by the SNX Council. This document was also sent out by PSI for international review and received excellent evaluations. The SNBL international beamline review panel in 2019 also strongly endorsed the project.

In brief, the new EBS source provides excellent opportunities for SNBL users. In order to materialize these opportunities, a 2-phase plan for SNBL was therefore developed and consequently approved to adapt and upgrade both beamlines to the new EBS source. *Phase 1 covers investments in beamline equipment that are directly induced by the new source characteristics of the ESRF-EBS upgrade (i.e. higher heat load on the optical components).* Phase 2 provides an evolving scientific case for both BM01 and BM31 and their proof of concept. Obviously, the equipment installed now for Phase 1 is already compatible with the future scientific goals of the Phase 2 upgrade.

Phase 1 being completely finished, the new contract period between the NTNU and EPFL started and 2 Million Euro’s external funding available Phase 2 was ready was start. Major design works have hence been undertaken for the development of the new BM31 end station. The prior conceptual work was transformed in a full technical design (Figure 1 and 2) and all parts were ordered and machined by external companies. The assembly has started in 2021 and will continue in 2022. The new detector for PDF was also acquired and will be integrated in the new setup.

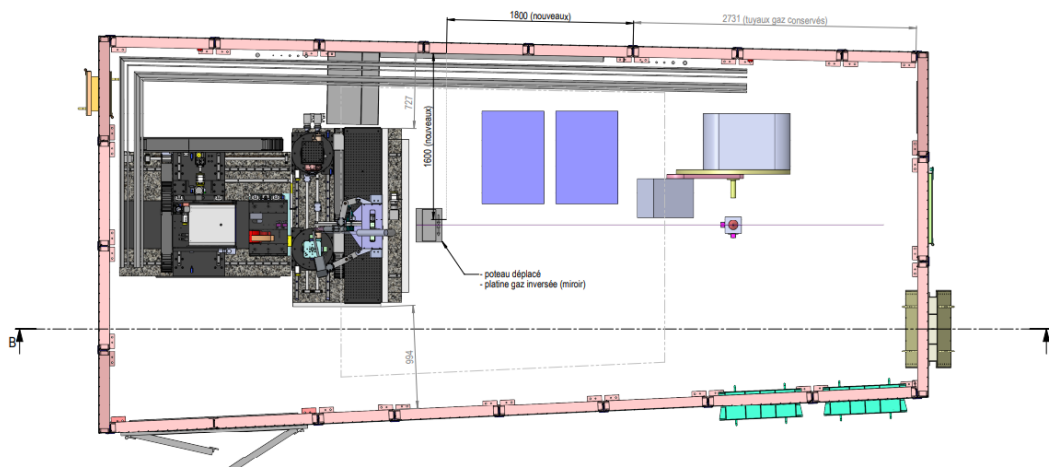


**Fig. 1:** Top view illustrating the layout of the upgraded experimental hutch of BM31. At the left side the new designed end-station XAFS-PDF-XRD.

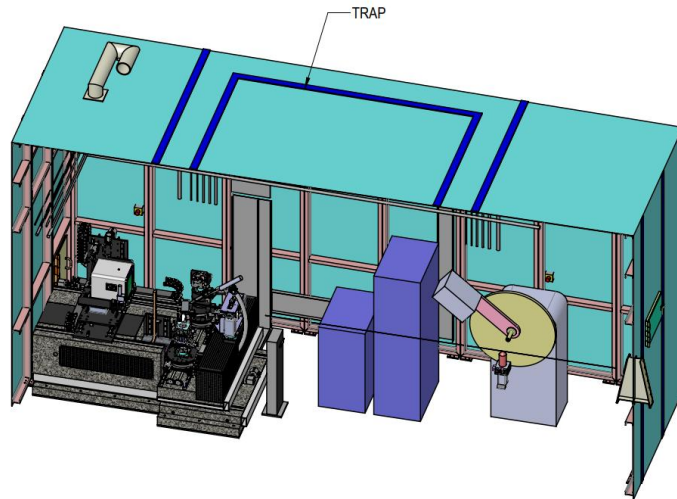


**Fig. 2:** Isometric view illustrating the layout of the upgraded experimental hutch of BM31. At the left side the new designed end-station.

On BM01 the major job to be done was the implementation of a second detector for SAXS. The detector has been acquired and a new frame was designed and orders for construction were placed. See figure 3.

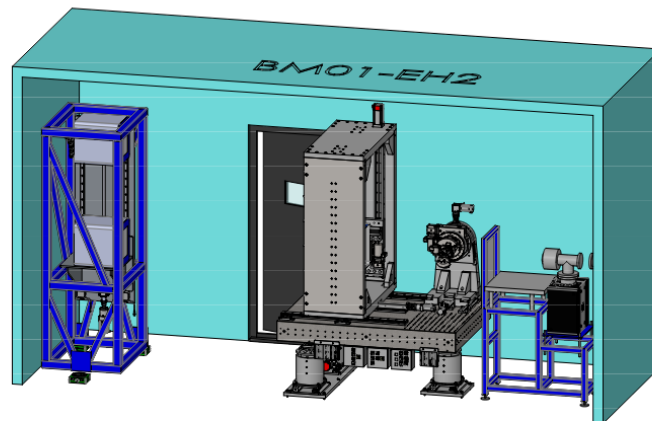


**Fig. 3:** Isometric view illustrating the layout of the upgraded experimental hutch of BM01. At the left side the new designed end-station for SAXS in the middle the existing end-station for XRD.